Comparison of Electromagnetic Performance of 10MW Superconducting Generators with Different...

Article *in* IEEE Transactions on Applied Superconductivity · July 2017

CITATIONS
0

READS
4

7 authors, including:

Guang-Jin Li
The University of Sheffield
42 PUBLICATIONS **274** CITATIONS

SEE PROFILE

Comparison of Electromagnetic Performance of 10MW Superconducting Generators with Different Topologies for Offshore Direct-Drive Wind Turbines

Y. Guan, Z. Q. Zhu, *Fellow, IEEE*, Ziad Azar, *Senior Member, IEEE*, A. S. Thomas, F. Vedreño-Santos, G. J. Li, *Senior Member*, *IEEE*, and M. Odavic

***Abstract*—This paper compares the electromagnetic performance of 10MW superconducting (SC) generators with three different topologies, i.e., iron-cored stator and rotor (ISIRT), iron-cored stator and air-cored rotor (ISART), and air-cored stator and rotor (ASART). The objective is to provide a powerful insight into the advantages and disadvantages of the different topologies, and to establish some design guidelines for selecting an appropriate direct drive SC generator for offshore wind turbine applications. Firstly, the structures of the three SC generator topologies are introduced. Then, the influence of the SC coil cross sectional area on torque capability is compared. After that, three SC generators with different topologies are optimized respectively for further comparison, including the active material cost, weight, harmonics in the electromotive force (EMF), torque ripple, field harmonics in the SC coil, and forces on the rotor and stator components, etc. It is found that, with the same SC quantity, the torque capability of the iron-cored stator and rotor topology is much better than that of the other two topologies. However, the advantage becomes less significant when a larger area of the SC coil is employed. The air gap flux density waveform of the ASART is much smoother than those of the ISIRT and ISART. The torque ripples of the ISIRT and the ISART are much higher than that of the ASART. The field harmonics (both amplitude and frequency) in the SC coil of the ASART are the lowest. For the ISIRT, most of the force on the rotor is acting on the rotor iron, and thus, the SC coil is more likely to be safe from a mechanical performance point of view and the design of the corresponding supporting structure is simple. However, for the air-cored rotor topologies, nearly all the force is acting on the SC coil. For the air-cored stator, the force mainly acts on the armature winding, while for the iron-cored stator, it is mainly on the stator teeth. Due to the excellent mechanical performance of iron, the iron-cored stator is therefore more robust.**

***Index Terms*—direct-drive, field harmonic, HTS, superconducting generator, wind turbine.**

The work is financially supported by the European Union's Seventh Framework Program for research, technological development and demonstration under grant agreement No. 308974, Project name: Innovative Wind Conversion Systems (10-20MW) For Offshore Applications (INNWIND).

Y. Guan, Z. Q. Zhu, F. Vedreño-Santos, G. J. Li, and M. Odavic are with Department of Electronic and Electrical Engineering, University of Sheffield, S1 3JD, UK (e-mail: {y.guan, Z.Q.Zhu, f.vedrenosantos, g.li, m.odavic}@sheffield.ac.uk)

Ziad Azar and A. S. Thomas are with Siemens Wind Power, Sheffield, S3 7HQ, UK (e-mail: {ziad.azar, arwyn.thomas}@siemens.com).

I. Introduction

Wind energy is developing rapidly, due to the concerns of greenhouse effects and conservation of fossil fuels. According to the installation location, wind turbines can be divided into onshore and offshore categories. The offshore wind turbine market is developing much faster than the onshore market, due to high average wind speed, limited onshore installation locations, less interference with habitants, and potentially shorter transmission distance between wind farms (power source) and densely populated cities (consumers) near the coast, resulting in reduced power losses and cost of power transmission, etc. [1] [2]. However, offshore wind turbines also have some disadvantages, such as difficulties of foundation, grid connections and maintenance, etc. In addition, much attention needs to be paid to the high reliability of wind turbines. Usually, direct-drive generators are preferred, because failure and maintenance of the gearbox are avoided [3]. Furthermore, a wind farm with a smaller number of large power wind turbines is preferable to that with many small ones. However, as the power of the wind turbines increases, the cost and installation difficulty do not increase linearly, mainly due to the limitation of the current available capacity (300 tons) of the offshore wind turbine installation vessel [4]. Currently, the cost and installation difficulty increase significantly for conventional offshore direct-drive generators, if the power is higher than 6~7MW [5].

The superconducting (SC) material has the capability of carrying large current densities, two orders of magnitude larger than that of copper. Thus, a large power SC generator can be realized with much lower weight and size, which makes it desirable for offshore wind turbine applications. The 10MW direct-drive SC generator designed by American Superconductor (AMSC) is ~150 to 180 tons, while the permanent magnet (PM) and copper field winding excited synchronous generators can be as heavy as 300 tons and 500 tons respectively [6]-[7].

According to the materials of the armature and field windings, SC generators can be divided into fully and partially

SC generators. The fully SC generator has SC material for both the armature and field windings. The partially SC generator employs SC material for the field winding and copper for the armature winding. Due to the immaturity of the SC material capable of carrying AC currents and working within AC fields, which causes high AC losses, the fully SC generator is still far from commercialization [8]. According to the material of the stator tooth and rotor pole, the partially SC generator can be further divided into three topologies, i.e., iron-cored stator and rotor topology (ISIRT), iron-cored stator and air-cored rotor topology (ISART), and air-cored stator and rotor topology (ASART). The partially SC generators can also be divided into three categories, i.e. low temperature SC (LTS), high temperature SC (HTS), and MgB_2 SC generators [9]-[10]. The LTS material has the lowest operation temperature (~4.2K), but the lowest price. The HTS material has the highest operation temperature (between 30K and 77K) and better mechanical performance. However, its price is the highest. The operating temperature of MgB_2 material is 15-20K, and its price is between those of LTS and HTS. In this paper, only the second generation (2G) HTS generators are analyzed.

The ASART is a good candidate for large-power offshore wind turbines due to its light weight, because a light non-magnetic material is used as the stator teeth and rotor poles instead of iron. A lot of research has been focused on this topology [11]-[14]. Compared with the ASART, iron is still used for the stator teeth of the ISART [15]-[16]. The mechanical performance of the iron-cored stator is much better due to the use of robust iron teeth [8]. Currently, the biggest challenge of the commercialization of the SC generator is the high price of the SC wire, especially the second generation (2G) of high temperature SC material. Consequently, the ISIRT has gained much attention in recent years [17]-[19] due to the relatively lower SC material consumption, although the weight is likely to be higher than that of the ISART and ASART [20]. The performance of different topologies is compared in literature, mainly in terms of cost and weight [20]-[22].

In this paper, a comprehensive comparison is carried out for the performance of the three partially SC generator topologies, in terms of torque capability, cost, weight, electromotive force (EMF), torque ripple, field harmonic in the SC coil, and force on the rotor and stator components, etc. The objective is to provide a powerful insight into the advantages and disadvantages of the different topologies, and to establish some design guidelines for selecting an appropriate topology for a range of applications. The main contributions include: (1) This paper investigates the influence of both the SC coil area and the materials (air or iron, i.e. air-cored or iron-cored) of teeth and yokes for the stator and the rotor on the torque capability. The ISIRT has significant advantages in terms of torque or power capability when less SC coil is used, but the advantage becomes less significant as the amount of SC material increases. This has not been reported in literature such as in [18]-[20]. (2) Moreover, the field harmonics within the SC coil due to armature and/or field currents are intensively investigated and compared for different generator topologies so as to predict their AC losses, and further the relative capability of maintaining the superconductivities of the SC coil under different operating conditions. The accurate prediction is out of the scope of this paper, since thermal analysis is needed. (3) In addition, the magnetic force on the stator and rotor components with a particular focus on the SC coils is also compared for different generator topologies. All these investigations will provide more in-depth and quantitative analyses in order to achieve better understanding of the different SC generator topologies. This paper is organized as follows. In section II, the structures of the three different SC generator topologies are described. Three SC generators are optimized and their torque (power) capabilities are compared in section III, whilst other performance indicators are compared in section IV, such as no load flux density, phase back-EMF, on-load torque, torque ripple, field harmonics in the SC coil, and force on the rotor and stator components, etc. The conclusion is given in section V.

II. SC Generator Structure

The structures of the SC generators with three different topologies are shown in Fig. 1. The stator of the ISIRT consists of an iron yoke and teeth, and a copper armature winding. The rotor consists of iron rotor poles and SC field winding. Usually, the SC coils can be either cooled together with the rotor iron (cold rotor topology), or cooled by itself (warm rotor topology). The cold rotor topology has a more stable cryogenic environment, due to the large thermal capacity caused by the rotor iron [8] and [23]. However, compared to the warm rotor topology, it has longer cool down time due to larger cold mass. Moreover, it should be mentioned that the active air gap length of the cold rotor topology should be longer, in order to accommodate the iron pole in a cryostat. For the above reasons, the ISIRT in this paper will only adopt the warm rotor topology while the ISART and ASART employ cold rotor topology. For the ISART, non-magnetic material (e.g. fiber reinforced plastic [4]), instead of iron, is used in the rotor pole, which is for the structural supporting and cooling of the SC coil. For the ASART, both the stator teeth and rotor poles are made of this non-magnetic material.

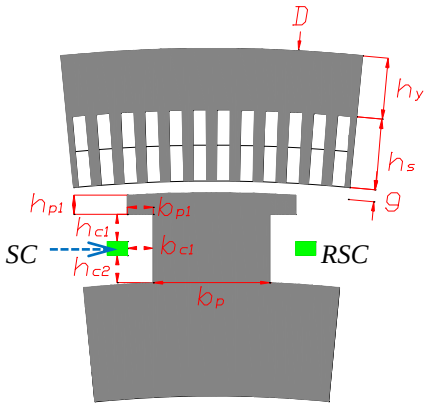

(a)

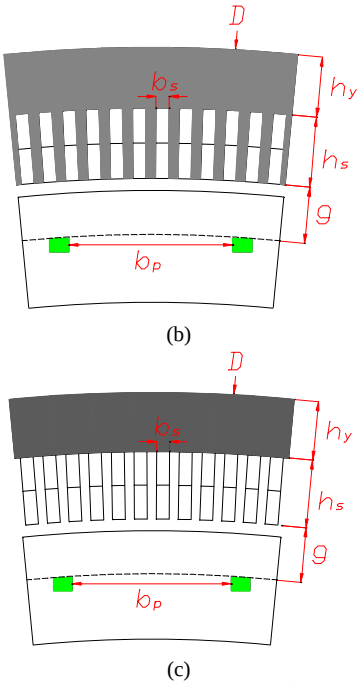

Fig. 1. Cross sections and dimensional parameters of SC generators. (a) ISIRT, (b) ISART, (c) ASART. D is the stator outer diameter, h_s is the stator yoke height, b_s and h_s are the stator slot width and height, g is the active air gap length, h_{p1} and b_{p1} are the rotor iron pole dimensions, b_{c1}, h_{c1} and h_{c2} are the distances between SC coil and rotor iron pole, b_p are the rotor iron pole width for the ISIRT and SC coil pitch for the ISART and ASART, *SC* and *RSC* are the two sides of the SC coil.

III. Comparison of Torque or Power Capability

A. Optimization Procedure

The torque or power capabilities of different topologies are firstly compared in this section. For a fair comparison, the stator outer diameter, stack length and pole number are set to be the same, which are 7m, 1.2m and 32 respectively. According to the investigation in [24], D=7m can provide good utilization of SC material and generator volume. More investigation about the influence of D on the generator weight will be conducted in the future in order to select an optimal D. All of the SC generators are optimized with the same stator DC copper loss, 525kW, and the electromagnetic torque is set to be the optimization target. During this process, the end winding loss is considered, and the method of calculating the end winding length can be found in [24]. However, the stator armature winding eddy current and circulating current losses, the stator iron losses, and the cryogenic system loss are neglected in order to simplify the optimization. In addition, the thermal performance of each topology is different. The ASART has the worst thermal performance, due to the lack of an iron core around the winding, which increases the operating temperature. Therefore, it may not be a completely fair comparison to assume equal stator copper losses. For each design, there are numerous dimensional parameters which can be optimized, as shown in Fig. 1. In order to further simplify the optimization process, the parameters related to the cryostat installation and fixing are determined in advance without optimization:

1) For the ISIRT, h_{p1}=40mm, b_{p1}=h_{c1}=h_{c2}=b_{c1}=60mm.

2) For the ISART and ASART, the distance between the stator and SC coil (active air gap length) g=82mm. The space between them is for the design of the cryostat and shield for the SC coil. This empirical value is appropriate for the initial design, and it can be adjusted after further detailed thermal analysis.

During the investigation, the distance between adjacent SC coils is not considered. It is possible that this distance may be very short and there is not enough space for mechanical support of the SC coil. More detailed mechanical and cryostat designs are needed and will be conducted in the future. The finite element software MAXWELL is utilized for the torque calculation and the zero d-axis current i_d=0 control is adopted [25]. The corresponding phasor diagram is shown in Fig. 2, in which the d-axis is aligned with the rotor field. The optimization process is shown in Fig. 3, which mainly consists of two steps, determination of S_{sc} and J_{sc} (step I), and optimization of D_i, b_s and h_s (step II). For step I, a SC coil operating current density, with a 25% safety margin compared to the critical current density, is always maintained in order to safely utilize the SC material. The 2G HTS YBCO, developed by Siemens Corporate Technology, is adopted for the design of the three topologies and the temperature is assumed to be 30K. The critical J-$B\perp$ characteristic of the HTS can be found in [24]. The optimization procedure and the process of determining the operating current density of the SC coil are shown in Fig. 3. $B\perp$ is the flux density perpendicular to the surface of the SC wire. The critical current density of the SC coil can be obtained according to the SC material J-$B\perp$ characteristic. A 25% safety margin is realized through an iterative process. For step II, the torque capability at 9.6rpm is calculated for a wide range of combinations of the stator inner diameter D_i, stator slot height and width h_s and b_s, and rotor pole width/SC coil pitch b_p. The combination which can achieve the maximum torque is determined as the final design. The parameters, D_i, h_s and b_s, are optimized all together. Because the MMF of stator winding is much lower than the SC coil MMF, the flux density within the SC coil is mainly affected by the SC coil area and J_{sc}. In that case, the determination of J_{sc} can be assumed to be independent of the stator. Consequently, the determination of J_{sc} is separated from the optimization of D_i, h_s and b_s.

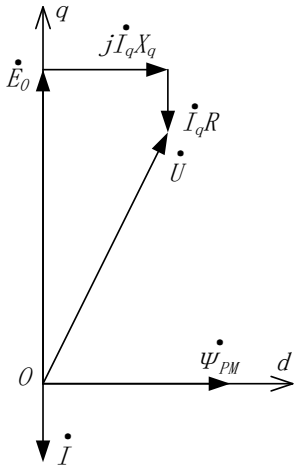

Fig. 2 Phasor diagram of $\dot{I}_d = 0$ control, $\dot{I}$ is the stator current vector, $\dot{I}_d$ and $\dot{I}_q$ are the d- and q-axis current vectors, $\dot{E}_0$ is the no-load back EMF, $\dot{U}$ is the stator voltage vector, R is the stator phase resistance, X_q is the q-axis reactance.

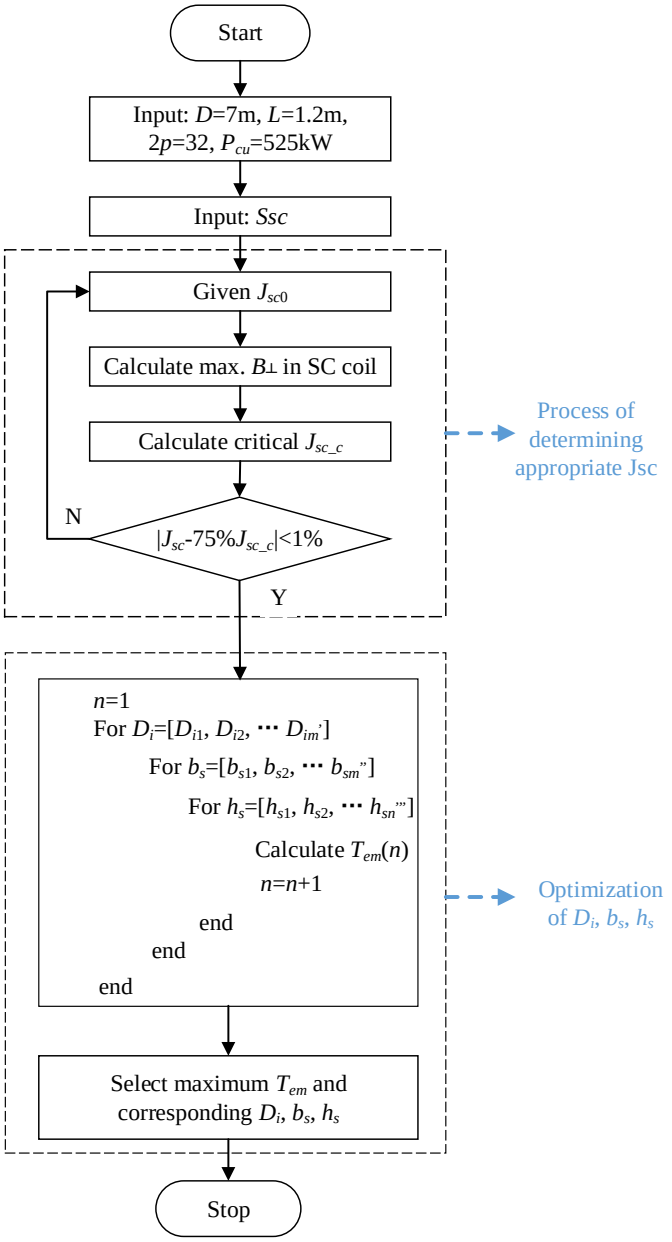

Fig. 3. Flow chart of the optimization process, D_i is the stator inner diameter.

B. *Comparison of Torque Capability*

For each SC generator with a different SC coil area, the optimization process, as shown in Fig. 3, is repeated and the maximum possible torque is obtained. The variations of the torque with the SC coil area (S_{SC}) for the three topologies are shown in Fig. 4. The torque capability of the ISIRT is the highest, since it uses the most iron material, which is favorable for reducing the reluctance of the main flux path, and hence increasing the air-gap flux density. The torque of the ISART is higher than that of the ASART. For the ISIRT, the torque increases with the SC coil area. However, after some point, the increase becomes saturated due to the saturation of the iron. For the ISIRT, the trend of the torque variation is similar to that of the *B-H* curve of the iron material. The similarity is clearer when the *x*-axis scale in Fig. 4 is reduced. The torque increases more linearly with the SC coil area in the ISART and ASART because less iron is used. Consequently, the ISIRT has significant advantages in terms of the torque capability when less SC coil is used, and the advantage becomes less significant when more SC material is used.

Nowadays, the high price of HTS material is an important threshold for the commercialization of SC generators, and a design with less HTS material is preferable. Consequently, the ISIRT is more popular from a cost point of view. As the price of the HTS material could reduce in the future, more HTS material can be used in the field winding, thus the ISART and ASART may be more preferable due to their lighter weight.

The critical and operating current densities of the SC coil are shown in Fig. 5. The critical current density of the SC coil is mainly influenced by the SC coil area rather than the generator topology. As the SC coil area increases, the critical current density decreases due to the increase of the excited maximum flux density in the SC coil. Therefore, a larger area of SC coil leads to a lower critical current density and operating current density. During the optimization process, again a 25% safety margin of the operating current density, with respect to the critical current density, is always kept.

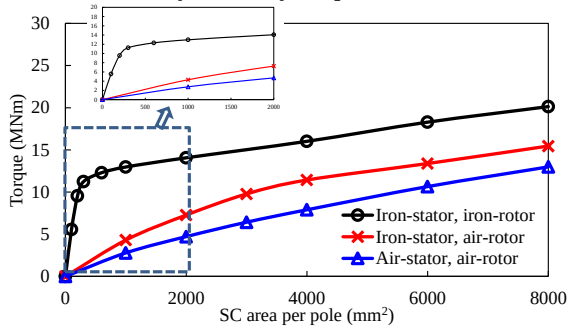

Fig. 4. Variations of torque with SC coil area per pole.

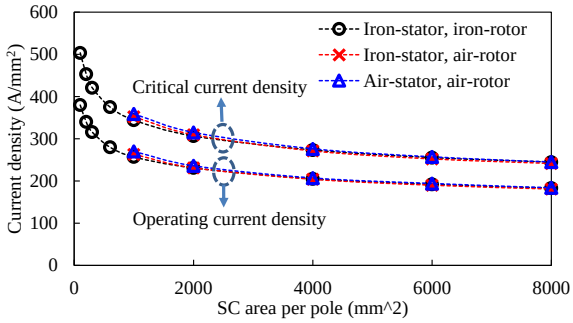

Fig. 5. Variations of SC coil critical and operating current densities with SC coil area per pole.

IV. Comparison of Other Performances

A. *Specification of the SC Generators*

For further comparison, three generators with different topologies are designed according to the specifications of 10MW offshore wind turbines, which are listed in TABLE I. The design objective is to achieve the maximum torque density, under the same copper loss condition. The optimized parameters include the SC coil cross section area S_{SC}, stator yoke thickness h_y, stator slot height and width h_s and b_s, and rotor pole width/SC coil pitch b_p.

The determination of the appropriate S_{SC} is a little complicated. The torque capability always increases with S_{SC}, as shown in Fig. 4. A larger S_{SC} is preferred from the generator volume point of view. However, it may be not economically feasible, due to the high cost of the HTS material. As can be

seen from Fig. 4, the increase in the torque capability with the SC coil area is saturated after a certain point. The appropriate SC coil area per pole can be determined around the saturation point. Finally, the SC coil areas per pole for the ISIRT, ISART, and ASART are determined as 200mm^2, 3000mm^2 and 6000mm^2 respectively. For the ISART and ASART, the proper SC coil areas are not easy to select, because there are no saturation points. In this case, 3000mm^2 and 6000mm^2 are determined to make the stack lengths of the three topologies and also the stator outside heat dissipation area similar. It is not appropriate to determine the SC coil area only from the torque density point of view. More comprehensive performance investigation needs to be taken into account. With further investigation on other performances, such as cryogenic system design, overall weight and cost and so on, the SC coil cross section may need to be adjusted. The stator outer diameter D is chosen to be 7m. As mentioned earlier, according to the investigation in [24], D=7m can provide good utilization of SC material and generator volume.

TABLE I
SPECIFICATIONS OF SC GENERATORS

	Iron-stator Iron-rotor	Iron-stator Air-rotor	Air-stator Air-rotor
Power (MW)	10		
Speed (rpm)	9.6		
Line voltage (Vrms)	3300		
Torque, based on efficiency=95% (MNm)	10.5		
Stator outer diameter D (m)	7		
Stack length L (m)	1.16	1.06	0.95
Number of poles	32		
Number of slots	384		
h_y (mm)	210	210	175
h_s (mm)	238	231	92.5
b_s (mm)	16	17.5	40
g (mm)	7	82	82
b_p (mm)	300	517	529
Area of SC coil per pole (mm^2)	200	3000	6000
Dimensions of SC coil (mm)	7.9×12.65	30.6×49	43.3×69.3
Dimensions of SC wire (mm)	9.99×0.225		
Stator current density J_a (A/mm^2)	3.5		
SC coil current density J_{SC} (A/mm^2)	345	217	194
Maximum normal flux density / corresponding critical current density of SC coil @30K	1.34T / 430A/mm^2	3.22T / 272A/mm^2	4.09T / 241A/mm^2
Packing factor	0.6		
Length of SC wire (km)	5.348	81.66	156.4
Weight of iron (t)	136.3	64.6	29.2
Weight of stator winding (t)	14.8	14.8	14.8
Type of SC material	YBCO		
Cost of SC (million €), quotation=100(or 20)€/m	0.534 (0.107)	8.166 (1.63)	15.64 (3.13)
Cost of copper (million €), quotation=7.5€/kg	0.111	0.111	0.111
Cost of iron (million €), based on quotation=0.8€/kg	0.108	0.0517	0.0233
Cost of total active material (million €), with SC quotation=100(or 20)€/m	0.764 (0.327)	8.328 (1.795)	15.77 (3.26)

The optimization process of the other parameters is as follows. For each topology, the torque per stack length is calculated for a wide range of combinations of h_y, h_s, b_s, and b_p. The generator with the combination which can achieve the maximum torque per stack length is determined as the final design. During the optimization, the stator copper loss is fixed to be 495kW, in order to satisfy the efficiency requirement (>95%), since the AC losses, iron loss, and cryogenic system loss are neglected. However, when all of the aforementioned losses are taken into account, it is possible that the final efficiency is below 95%. Then a re-optimization with a lower stator copper loss is needed. More detailed analysis of the AC losses, iron loss and cryogenic system loss is out of the scope of the paper. It should also be mentioned that stator copper loss is kept to be 495kW in this section, which is different from the value 525kW in section III. The reason is that the generators optimized in this section have a smaller stack length, as listed in TABLE I, than 1.2m in section III. By assuming a higher copper loss for a longer stack length, the thermal loading can be kept similar, which allows a similar heat dissipation capability to be maintained. The optimization process is similar to that shown in Fig. 3. However, the difference is that the stack length is obtained using the target torque divided by the torque per stack length, not as an input parameter, because the generator needs to output the exact target torque or power. The single-objective (torque density) optimization strategy is adopted in this paper. Multi-objective (volume, weight and cost) optimization methods, such as AHP, PSO etc., will be considered in the future. The specifications of the optimized generators are listed in TABLE I.

The ISIRT uses less than 10% of the HTS material used in the ISART. Consequently, the total active material cost is the lowest, less than 10% of the cost of the ISART, with the HTS quotation=100€/m. The quotations of HTS, the prices of iron and copper were provided by the Siemens suppliers. It is believed that the HTS price will reduce significantly in the future. If the HTS quotation=20€/m, the total active material cost of the ISIRT is still less than 20% of other topologies. Because the iron is used as the rotor pole, the iron weight of the ISIRT is about twice of the weight of the ISART. The ASART has the highest cost and lightest iron weight, approximately twice of the cost and half of the weight of the ISART respectively. For the ASART, the costs of HTS material, copper and iron is ~10, ~0.1 and ~0.023 million €, which are at the similar levels as that shown in [26]. Because only the electromagnetic design is carried out, only the weight and costs of active material are considered. The weight and costs of other components, such as the supporting structure and cryogenic system etc., are not included in TABLE I. The nonmagnetic material cost could be significant, and more detailed investigation will be conducted in the future to provide fairer comparisons for weights and costs.

It should be mentioned that the cooling of the armature winding could be problematic due to the high electrical loadings of these designs, e.g. about 160kA/m for the ISIRT. The thermal constraints could not be met. It is therefore likely that the water cooling or forced-air cooling method (with air flow goes through the stator slots and acts on the armature winding directly) would be needed, [27]. However this is out of the scope of this paper, it is therefore not included.

B. *No load Flux Density and Phase EMF*

The no-load waveforms and spectra of flux density in the middle of the air gap and phase EMF are shown in Fig. 6 and Fig. 7.

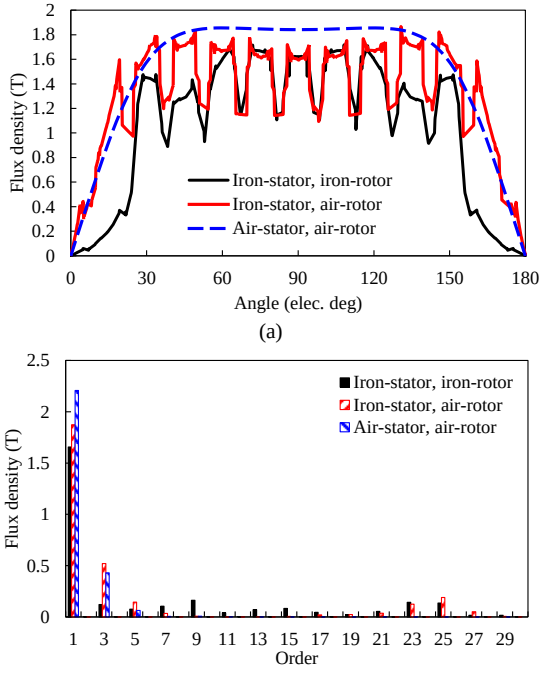

Fig. 6. No load flux density in the air gap. (a) Waveforms. (b) Spectra.

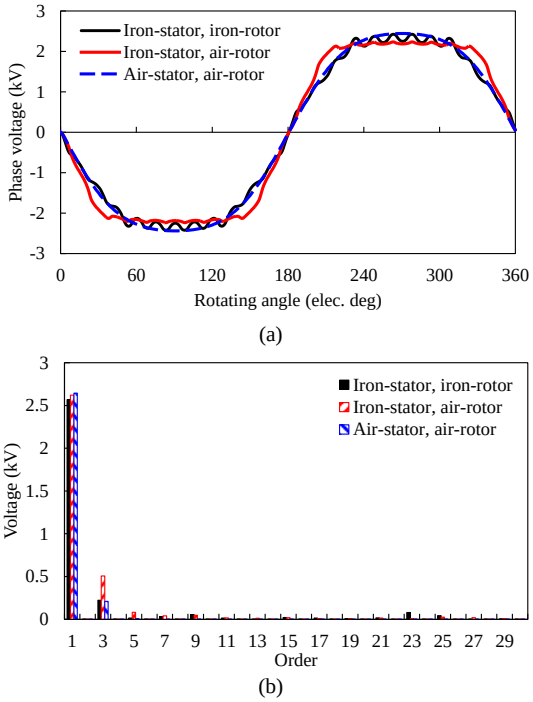

Fig. 7. Phase EMF. (a) Waveforms. (b) Spectra.

The waveforms of the ASART are the smoothest, without the influence of the stator iron teeth. The average air gap flux density level is 1.5-2T, much higher than that of the conventional PM topologies, ~1T. The magnitude of the third harmonic for the ISIRT is lowest, due to the influence of the pole shoe, which concentrates more flux in the middle of the pole. However, it contains rich higher order harmonics due to slotting effects, leading to much more distorted flux density waveforms. For the back-EMF, the waveform of the ASART is the smoothest, because the effect of the iron-teeth is removed.

C. *On-Load Torque and Torque Ripple*

The variations of average torque with stator current density are shown in Fig. 8(a). The increases in torque for the ASART and ISART are more linear than that of the ISIR. The torque increase for the ISIRT tends to be saturated after a certain point, because of the significant use of iron in the magnetic circuit. The torques of ISART and ASART are higher than that of ISIRT because the SC quantities are much higher. However, the results when the same amount of SC material is used are shown in Fig. 4. The waveforms and spectra of the rated torque are shown in Fig. 8 (b) and (c). The amplitudes of the torque ripple for the ISIRT and ISART are much higher than those of the ASART. The major torque ripple harmonic for the ASART and ISART is the 6th. However, the major harmonics for ISIRT are the 6th and 24th. The 6th torque harmonic is due to the interaction between the 5th and 7th harmonics of both the stator armature magneto motive force (MMF) and the rotor field. When the iron is used as the stator teeth, the 6th harmonic amplitude is increased significantly. This torque ripple can be reduced by employing techniques such as short-pitch winding and stator or rotor skewing, etc.

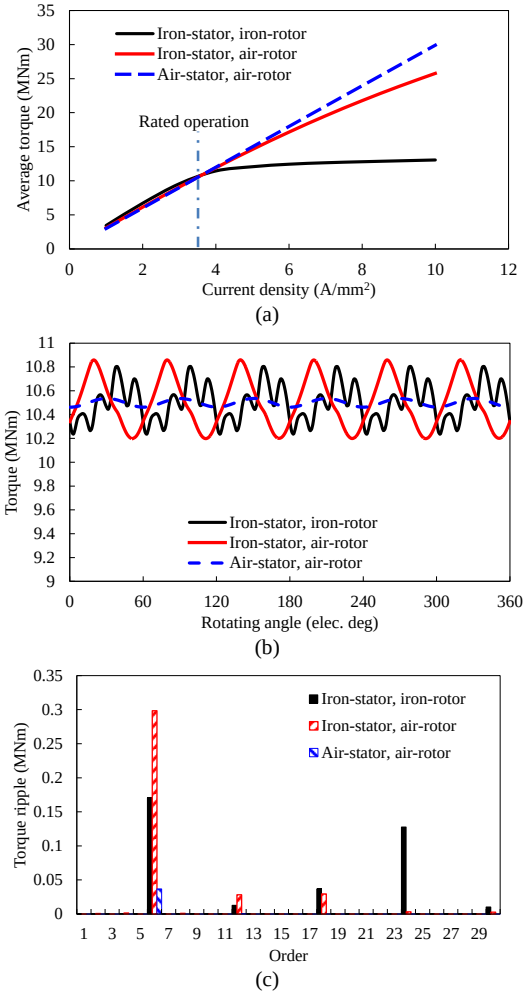

Fig. 8. Torque. (a) Variation of average torque with stator current density. (b) Waveforms of rated torque. (c) Spectra of rated torque.

D. Field Harmonics in the SC Coil

The superconducting status of the HTS tape is vulnerable to the produced heat within it. Thus, the induced varying flux density in the SC coil may be very large, thus producing AC losses. In this section, the induced field harmonics in the SC coil are analyzed, and the analysis is conducted for three different cases: (1) the field current is supplied and the armature current is zero; (2) the armature current is supplied and the field current is zero; (3) both the field and armature currents are supplied.

1) Field Harmonics in the SC Coil with the Armature Open-Circuited

The flux line distribution due to field current excitation only (the armature is open-circuited) is shown in Fig. 9. By way of example, the induced flux density variation with time or rotating angle at point A within the SC coil will be analyzed. The DC component in the flux density for the three topologies is quite different, with the ASART being the highest while the ISIRT being the lowest, Fig. 10 (a). The flux density waveforms and spectra are shown in Fig. 10 (b) and (c), with the DC components removed for a clearer comparison. For the ISIRT and ISART, there are only the 24th order harmonics within the SC coil, which is due to the influence of the stator iron teeth. For the ASART, there is nearly no varying flux density.

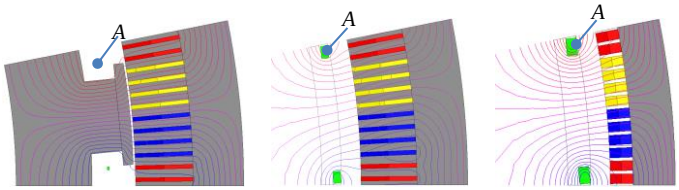

(a) (b) (c)

Fig. 9. Flux lines of the (a) ISIRT (J_a=0, J_{SC}=345A/mm^2), (b) ISART (J_a=0, J_{SC}=217A/mm^2) and (c) ASART (J_a=0, J_{SC}=194A/mm^2).

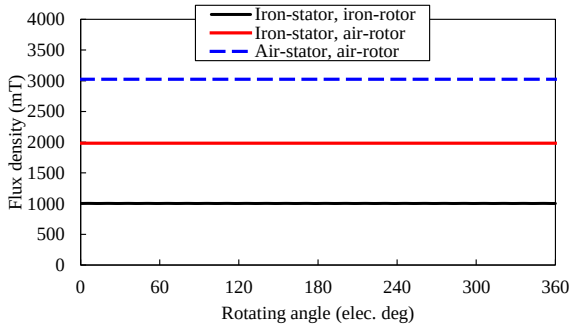

(a)

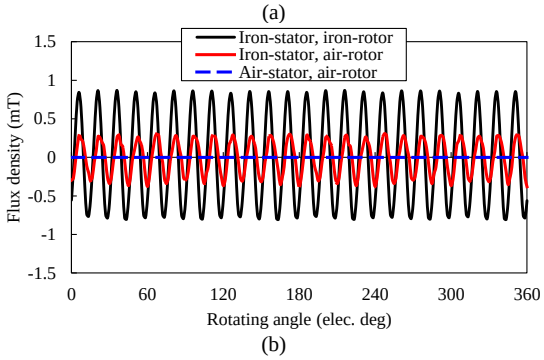

(b)

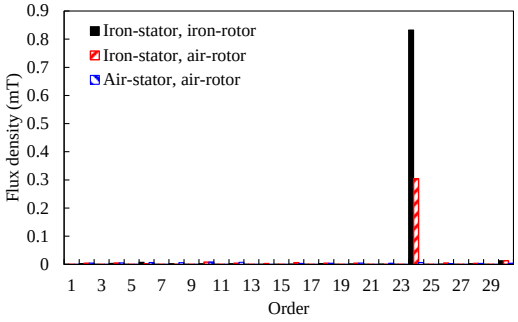

(c)

Fig. 10. Varying flux density at point A in the SC coil due to field current only with armature open-circuited. (a) Waveforms. (b) Waveforms, with DC components removed. (b) Spectra.

2) Field Harmonics in the SC Coil due to Armature Current with the Field Winding Open-circuited

When only the armature current is supplied, the flux lines are shown in Fig. 11. The induced varying flux density at point A in the SC coil is shown in Fig. 12.

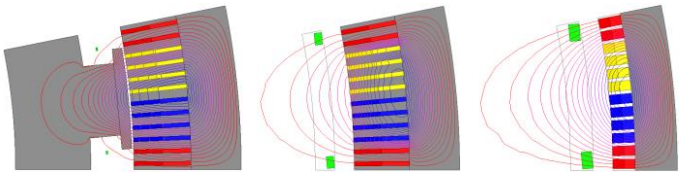

(a) (b) (c)

Fig. 11. Flux lines of the (a) ISIRT, (b) ISART and (c) ASART, J_a=3.5A/mm^2, J_{SC}=0.

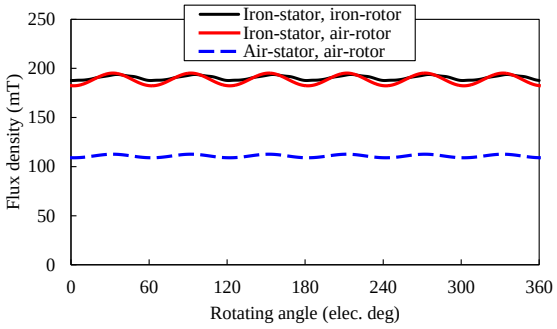

(a)

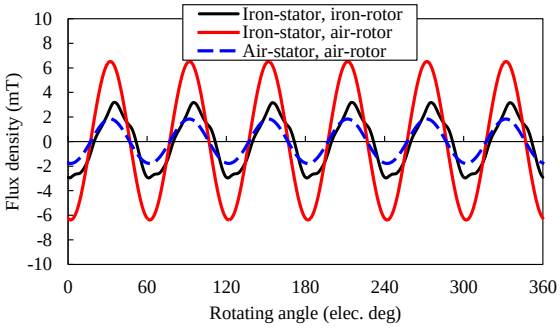

(b)

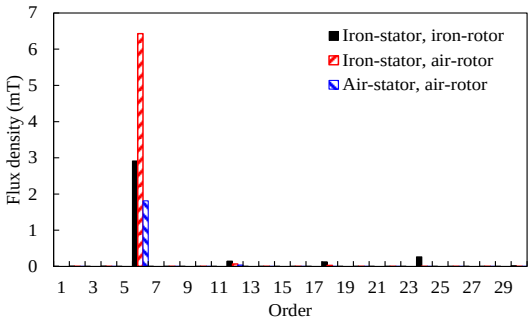

(c)

Fig. 12. Varying flux density at point A in the SC coil, with only armature current supplied and the field winding open-circuited. (a) Waveforms. (b) Waveforms, with DC components removed. (c) Spectra.

The major flux density harmonic is the 6th, which is caused by the 6th stator phase belt MMF harmonic. As can be seen from Fig. 11 (a), the iron-cored rotor forces more flux lines to go through the rotor pole instead of the SC coil, which is favorable to reduce the field harmonics in the SC coil. The air-cored stator is also favored to reduce the influence of the armature current on the field winding, due to the increased reluctance between the armature and field windings. Consequently, the induced field harmonics in the SC coil for the ISART are the highest, as shown in Fig. 12.

3) Field Harmonics in the SC Coil due to Both Armature and Field Currents

When both the armature and field currents are supplied, the flux lines and induced varying flux density in the SC coil are shown in Fig. 13 and Fig. 14, respectively.

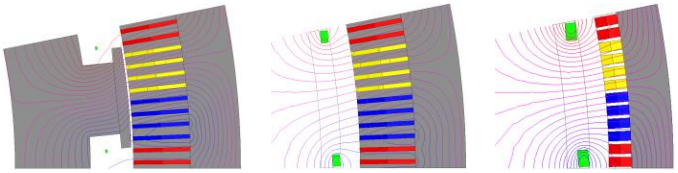

(a) (b) (c)

Fig. 13. Flux lines of the (a) ISIRT (J_a=3.5A/mm^2, J_{SC}=345A/mm^2), (b) ISART (J_a=3.5A/mm^2, J_{SC}=217A/mm^2) and (c) ASART (J_a=3.5A/mm^2, J_{SC}=194A/mm^2).

The major field harmonics for the ISIRT are the 6th and 24th, which are due to the 6th stator MMF harmonic and the influence of the stator iron-teeth, respectively. Although the amplitude of the 24th harmonic is lower than the 6th harmonic, the frequency is much higher, which may cause more AC losses (heat) in the SC coil. The major harmonic for the ISART is the 6th, which is highest amongst the three topologies. Overall, the field harmonics for the ASART are the lowest, with only comparable 6th harmonic.

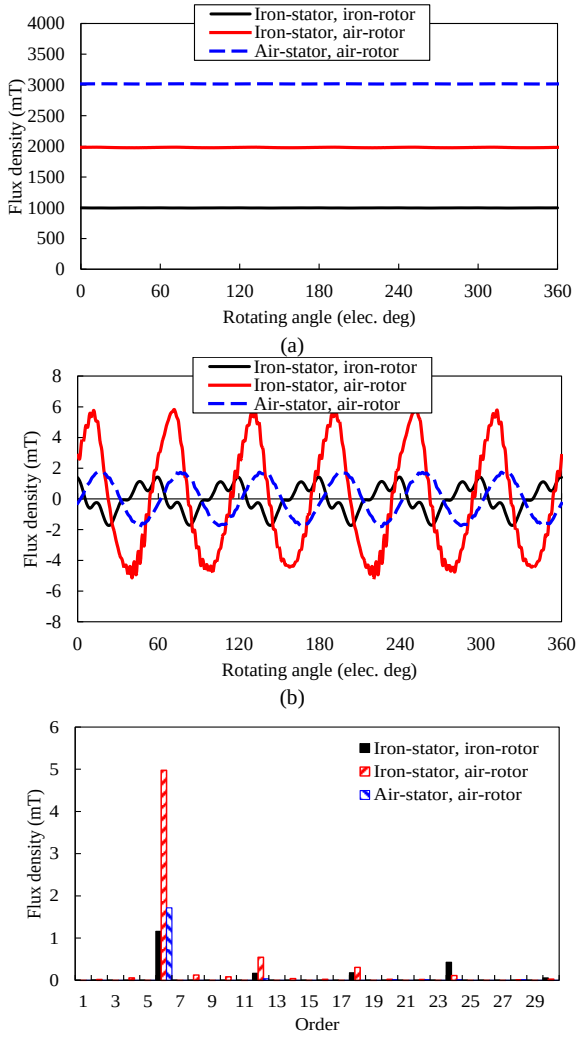

(a) (b) (c)

Fig. 14. Varying flux density at point A in the SC coil, with both armature and field currents imposed. (a) Waveforms. (b) Waveforms, with DC components removed. (c) Spectra.

E. Force on the Rotor Components

The mechanical performance is an important criterion for manufacturing the HTS tape, and a lot of effort has been focused on improving it in order to promote its commercialization. During the design of the SC generators, a smaller force on the SC material is preferable in order to protect the SC material and to simplify the supporting structure. In this section, the force on the rotor components is analyzed. The force for each separated part can be calculated according to the Maxwell Stress and the flux density vectors along a closed loop with only the separated part inside. The radial and tangential force densities can be expressed as:

$$f_r = \frac{1}{2\mu_0}(B_r^2 - B_t^2) \quad (1)$$

$$f_t = \frac{1}{2\mu_0} 2B_r B_t \quad (2)$$

where μ_0 is the vacuum permeability, B_r and B_t are the radial and tangential flux densities.

The analyzed rotor components include the SC coil and rotor iron, and the forces along the radial and tangential directions are calculated respectively. The force vectors on different rotor components can be easily obtained by utilizing the FEA. The

force calculation is carried out for a fractional part of the whole generator (1/32 of the whole generator), involving one SC coil and one rotor iron pole. The forces on the rotor components are shown in Fig. 15. For the ISIRT, most of the force is acting on the rotor iron. Thus, the SC coil is more likely to be safe from a mechanic point of view and the design of the corresponding supporting structure is simple, than the other two topologies. However, in the air-cored rotor topology, nearly all the force is acting on the SC coil. Thus, there is an increased requirement for the mechanical performance of the SC coil and the design of the torque transfer component is much more challenging. It can also be seen that for both the SC coil and the rotor iron, the radial force F_r is much larger than the tangential force F_Θ.

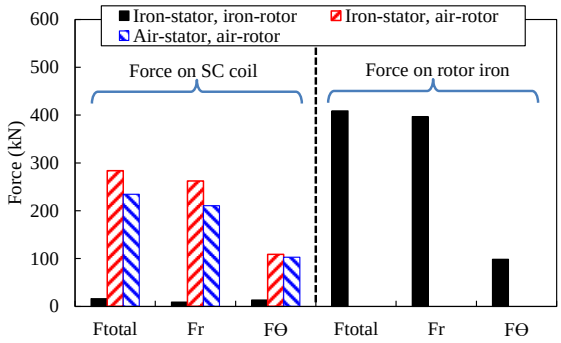

Fig. 15. Force on rotor components, F_{total} is the total force. F_r and F_Θ are radial and tangential force components.

The forces on the two straight parts of the SC coil (SC and RSC, as defined in Fig. 1 (a)) and rotor iron, are listed in TABLE II. The major forces on the SC and RSC are both along the tangential directions, but their directions are opposite and tend to increase the span of the SC coil. The difference between the two forces is utilized to produce the electromagnetic torque. It should be mentioned that, the total forces on the two sides of the SC coil of the ASART are very high, 954.5kN and 856.1kN respectively, as shown in TABLE II. However, due to the opposite direction of their tangential components, the total force on the whole SC coil is only 234kN, as shown in Fig. 15. In addition, the force on SC is larger than that on RSC, because the flux density around SC is higher than that around RSC, as shown in Fig. 13.

TABLE II
FORCES ON ROTOR COMPONENTS

		F_{total}(kN)	F_r(kN)	F_Θ(kN)
Iron-stator, iron-rotor	SC	11.95	-7.97	8.89
	RSC	4.75	-0.87	4.67
	Rotor iron	409	396.9	98.6
Iron-stator, air-rotor	SC	492.8	115.4	479.1
	RSC	398.6	146.7	-370.6
Air-stator, air-rotor	SC	954.4	89.5	950.1
	RSC	856.1	121.0	-847.5

F. Force on the Stator Components

The force on the stator components under rated operating conditions is analyzed in this section. Again, the calculation is conducted for 1/32 of the whole stator, consisting of 12 teeth and armature conductors in 12 slots. The forces on the armature winding and stator tooth are shown in Fig. 16 and TABLE III. For the air-cored stator, all of the force is on the armature winding, and it is mainly along the tangential direction, which is utilized to produce the electromagnetic torque. For the ISIRT and ISART, the major force is acting on the iron-teeth. The force on the iron-teeth along the radial direction is larger than that along the tangential direction, and the direction is towards the rotor side. The force on the armature winding is negligibly small. Due to the excellent mechanical performance of the iron, the iron-cored stator is more robust than the air-cored stator.

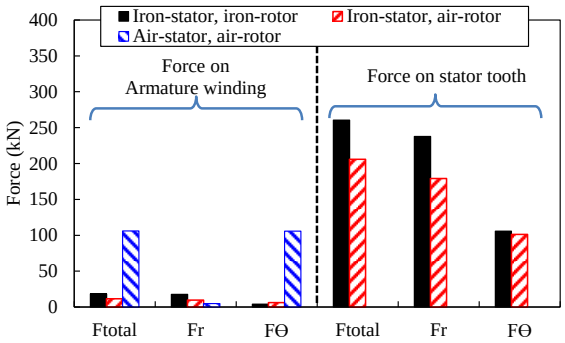

Fig. 16. Forces on stator components.

TABLE III
FORCES ON STATOR COMPONENTS

		F_{total}(kN)	F_r(kN)	F_Θ(kN)
Iron-stator iron-rotor	Winding	18.2	17.8	-4.1
	Stator tooth	260.3	237.8	-105.7
Iron-stator air-rotor	Winding	11.4	9.52	6.13
	Stator tooth	205.8	179.1	-101.2
Air-stator air-rotor	Winding	105.9	4.96	-105.7
	Stator tooth	0	0	0

V. CONCLUSION

In this paper, the performance of SC generators with three different topologies, i.e., ISIRT, ISART and ASART, are compared. The analyzed performance includes the torque capability, torque ripple, EMF, field harmonics in the SC coil, and forces on the rotor and stator components, etc. The ISIRT has significant advantages in terms of torque or power capability when less SC coil is used, but the advantage becomes less significant as the amount of SC material increases. Consequently, when the price of the SC material is high, the ISIRT is more promising from a cost point of view. As SC material price reduces, the ISART and ASART may be preferable due to their lower weights. The comparison of the three designed SC generators show that the total active material cost of the ISIRT is less than 10% of that of the ISART, with the HTS quotation=100€/m, and the weight is about twice of the other topologies. The torque ripples of the ISIRT and ISART are much higher than that of the ASART. The field harmonics (both amplitude and frequency) in the SC coil of the ASART are the lowest. For the ISIRT, most of the force on the rotor is acting on the rotor iron, and thus, the SC coil is more likely to be safe from a mechanical performance point of view and the design of the corresponding supporting structure is simple. However, for the air-cored rotor topologies, all of the force is acting on the SC coil, and the major forces on its two straight parts are along opposite directions, which tend to increase its span. For the air-cored stator, the force is mainly

focused on the armature winding, while for the iron-cored stator, it is mainly on the stator teeth. Due to the excellent mechanical performance of iron, the iron-cored stator is therefore more robust. Because the current price of HTS is very high, the ISIRT topology is therefore more suitable for the offshore wind turbine application. However, more attention should be paid to its torque ripple and SC coil screening issue. The ISART and ASART topologies are more suitable for applications where the generator weight limitation is very tough. Meanwhile, the SC material price should be low enough to get the investment back and the mechanical performance is good enough to protect the SC coil from large force.

VI. References

[1] A. Zervos and C. Kjaer. (Mar. 2008). *Pure power: wind energy scenarios up to 2030*. [Online]. Available: www.ewea.org.

[2] A.B. Abrahamsen, N. Mijatovic, E. Seiler, T. Zirngibl, C. Træholt, P.B. Nørgård, N.F. Pedersen, N.H. Andersen, and J. Østergård, "Superconducting wind turbine generators," *Supercond. Sci. Technol*., vol. 23, p. 034019, 2010.

[3] H. Polinder, J. A. Ferreira, B. B. Jensen, A. B. Abrahamsen, K. Atallah, and R. A. McMahon, "Trends in wind turbine generator systems," *IEEE Trans. Emerg. Sel. Topics Power Electron*., vol. 1, no. 3, pp. 174-185, Sep. 2013.

[4] M. E. Khalil, "High temperature superconducting generator design for offshore wind turbine application," *2015 Int. Conf. Electrical Engineering and Information Communication Technology*, May 2015, pp. 1-6.

[5] M. Zhang and J. Patel. (2016). *High temperature superconducting (HTS) machines* [Online]. Available: http://ukmagsoc.rog/events/machiens.

[6] V. Prince. (2015). *Large-scale wind energy systems: 10MW and beyond*. [Online]. Available: http://www.magnetlab.com.

[7] G. Snitchler, B. Gamble, C. King, and P. Winn, "10MW class superconductor wind turbine generators," *IEEE Trans. Appl. Supercond*., vol. 21, no. 3, pp. 1089-1092, Jun. 2011.

[8] R. H. Qu, Y. Z. Liu, and J. Wang, "Review of superconducting generator topologies for direct-drive wind turbines," *IEEE Trans. Appl. Supercond*., vol. 23, no. 3, pp. 5201108, Jun. 2013.

[9] I. Marino, A. Pujana, G. Sarmiento, S. Sanz, J. M. Merino, M. Tropeano, J. Sun, and T. Canosa, "Lightweight MgB_2 superconducting 10MW wind generator," *Supercond. Sci. Technol*., vol. 29, no. 2, 2015.

[10] P. J. Masson. "Wind turbine generators: beyond the 10MW frontier," *in Symposium on Superconducting Devices for Wind Energy Systems*, pp. 1-8, 2011.

[11] S. Fukui, J. Ogawa, T. Sato, O. Tsukamoto, N. Kashima, and S. Nagaya, "Study of 10 mw-class wind turbine synchronous generators with HTS field windings," *IEEE Trans. Appl. Supercond*., vol. 21, no. 3, pp. 1151-1154, Jun. 2011.

[12] H. J. Sung *et al.*, "Practical design of a 10 MW class superconducting wind power generator considering weight issue," *IEEE Trans. Appl. Supercond.*, vol. 23, no. 3, p. 5201805, Jun. 2013.

[13] M. F. Hsieh, C. K. Lin, and I. H. Lin, "Design and analysis of high temperature superconducting generator for offshore wind turbines," *IEEE Trans. Magn.*, vol. 49, no. 5, pp. 1881-1884, May 2013.

[14] R. Shafaie and M. Kalantar, "Design of a 10-MW-class wind turbine HTS synchronous generator with optimized field winding," *IEEE Trans. Appl. Supercond.*, vol. 23, no. 3, p. 5202307, Aug. 2013.

[15] J. Wang et al., "Design of a superconducting synchronous generator with LTS field windings for 12 MW offshore direct-drive wind turbines," *IEEE Trans. Ind. Electron*, vol. 63, no. 3, pp. 1618-1628, Mar. 2016.

[16] R. Fair, "Superconductivity for large scale wind turbines," General Electric—Global Research/DUNS No. 086188401, Niskayuna, NY, USA, Final Sci. Rep.—DE-EE0005143, 2012.

[17] Y. Xu, N. Maki, and M. Izumi, "Electrical design study of 10-mw salient-pole wind turbine HTS synchronous generators," *IEEE Trans. Appl. Supercond*., vol. 24, no. 6, pp. 5202706, Dec. 2014.

[18] J. Lloberas, "Finite-element analysis of a 15-MW high-temperature superconductor synchronous generator for offshore wind energy applications," *IEEE Trans. Appl. Supercond*., vol. 25, no. 6, pp. 5204107, Dec. 2015.

[19] H. Karmaker and E. Chen, "Design concepts for a direct drive wind generator using new superconductors," *Conf. Electrical Power and Energy*, 2015, pp. 22-25.

[20] H. Karmaker, M. Ho, E. Chen, and D. Kulkarni, "Direct drive HTS wind generator design for commercial applications," *2014 Int. Conf. Electrical Machines*, Sept. 2014, pp. 491-495.

[21] Y. L. Liu, R. H. Qu, and J. Wang, "Comparative analysis on superconducting direct-drive wind generators with iron teeth and air-gap winding," *IEEE Trans. Appl. Supercond*., vol. 24, no. 3, pp. 1-5, Jun. 2014.

[22] Y. Terao, M. Sekino and H. Ohsaki, "Comparison of conventional and superconducting generator concepts for offshore wind turbines," *IEEE Trans. Appl. Supercond*., vol. 23, no. 3, p. 5200904, Jun. 2013.

[23] G. Klaus, M. Kilke, J. Frauenhofer, W. Nick, and H. W. Neumuller, "Design challenges and benefits of HTS synchronous machines," *IEEE 2007 Power Engineering Society General Meeting*, 2007, pp. 1-8.

[24] Y. Guan, Z. Q. Zhu, G. J. Li, Ziad Azar, A. S. Thomas, F. Vedreño-Santos, and M. Odavic. "Influence of pole number and stator outer diameter on performance of superconducting generator with iron-cored rotor topology for wind turbines," submitted to *IEEE Trans. Appl. Supercond*. for publication.

[25] N. Bianchi and S. Bolognani, "Unified approach to the analysis and design of an AC motor drive for flux-weakening operations," in *Rec. 33rd IEEE IAS Annu. Meeting Industry Applications Conf*., 1998, pp. 95–102.

[26] R. Shafaie, F. Amirkhanloo, and M. Kalantar, "Toward an optimum design of large-scale HTS synchronous generator for wind turbine applications," *IEEE Trans. Appl. Supercond*., vol. 26, no. 2, p. 5201408, Mar. 2016.

[27] C. Lewis and J. Muller, "A direct drive wind turbine HTS generator," *Proc. IEEE Power Eng. Soc. Gen. Meeting*, 2007, pp. 1-8.

VII. Biographies

Y. Guan received the B.Eng. and M.Sc. degrees from Zhejiang University, Hangzhou, China, in 2006 and 2008, respectively, and the Ph.D. degree from The University of Sheffield, Sheffield, U.K., in 2015, all in electrical and electronic engineering.

From 2008 to 2011, he was an Engineer with Sany Electrics Co. Ltd., Beijing, China. Since 2014, he has been a Research Associate with The University of Sheffield, Sheffield, U.K. His research interests include the design and analysis of permanent-magnet and induction machines, and superconducting generators.

Z. Q. Zhu (M'90–SM'00–F'09) received the B.Eng. and M.Sc. degrees from Zhejiang University, Hangzhou, China, in 1982 and 1984, respectively, and the Ph.D. degree from The University of Sheffield, Sheffield, U.K., in 1991, all in electrical and electronic engineering.

From 1984 to 1988, he lectured in the Department of Electrical Engineering, Zhejiang University. Since 1988, he has been with The University of Sheffield, where since 2000, he has been a Professor of electrical machines and control systems with the Department of Electronic and Electrical Engineering, University of Sheffield, and where he is currently the Head of the Electrical Machines and Drives Research Group and the Royal Academy of Engineering/Siemens Research Chair. He is also currently the Academic Director of Sheffield–Siemens Wind Power Research Centre (S^2WP), the Director of CRRC Electric Drives Technology Research Centre, Sheffield, U.K., and the Adjunct Director of Midea Welling Shanghai Electrical Machines Research Centre, Shanghai, China. His current major research interests include the design and control of permanent-magnet brushless machines and drives for applications ranging from automotive and domestic appliance to renewable energy. He is a Fellow of Royal Academy of Engineering.

Ziad Azar (M'11-SM'15) received the B.Eng. degree in electrical engineering from the University of Damascus, Damascus, Syria, in 2003 and the M.Sc. degree in electronic and electrical engineering and the Ph.D. degree in electrical engineering from The University of Sheffield, Sheffield, U.K., in 2008 and 2012, respectively.

His major research interests during his Ph.D. studies included the modelling, design, and analysis of permanent-magnet and magnetless brushless machines for automotive applications. Since 2012, he has been an Advanced Electromagnetic Design Engineer with Siemens Wind Power, Sheffield, U.K.

A. S. Thomas received the M.Eng. and Ph.D. degrees in electrical engineering from The University of Sheffield, Sheffield, U.K., in 2005 and 2009,

respectively. The topic of his Ph.D. thesis was motor/generator design for aerospace applications in collaboration with Rolls-Royce.
In 2009, he joined Siemens Plc. as a Development Engineer specializing in direct-drive permanent magnet generators for offshore wind turbines located in the Sheffield Siemens Wind Power Research Centre, Sheffield, where he is currently the Team Leader in the Department of Generator Research and Development, where research is conducted in all aspects of electrical machine design and control in collaboration with The University of Sheffield.

F. Vedreño-Santos received the M.Sc degree in electrical engineering in 2008, the M.Sc in renewable energies in 2012 and the PhD. degree in electrical engineering in 2013, from Universidad Politecnica de Valencia, Valencia (Spain).
From 2011 to 2013, he worked as Junior Researcher in several European institutions, such as Université Picardie-Jules Verne, Amiens (France), École Centrale de Nantes, Nantes (France) and the Austrian Institute of Technology, Vienna (Austria). In 2014, he joined the University of Sheffield, Sheffield (UK), as Research Associate in electrical machines in collaboration with the Sheffield Siemens Wind Power Research Centre (S2WP). His research interests include diagnostics and condition monitoring of electric machines and design and control of power electronics for wind power applications.

G. J. Li (M'11-SM'16) was born in Xiaogan, China, in 1984. He received the B.Eng. and M.Sc. degrees in electrical and electronic engineering from Wuhan University, Wuhan, China, in 2007 and University Paris XI, Paris, France, in 2008, respectively, and the PhD degree in electrical engineering from the Ecole Normale Supérieure de Cachan (ENS Cachan, France), in 2011.
Since 2012, he has been with The University of Sheffield, where he was initially a Research Associate in collaboration with Sheffield Siemens Wind Power Research Centre, Sheffield, and was subsequently appointed to a lecturer post in electrical machines since 2013. His main research interests include the design, the thermal and fault based analysis of switched reluctance machines and different permanent magnet machines.

Milijana Odavic (M'13**)** received the M.Sc. degree in electrical and electronic engineering from the University of Zagreb, Zagreb, Croatia, in 2004 and the Ph.D. degree from the University of Nottingham, Nottingham, U.K., in 2008.
In 2013, she became a Lecturer in Power Electronics in the Electronic and Electrical Engineering Department at the University of Sheffield, Sheffield, U.K. Prior to joining the University of Sheffield, she was a Research Fellow in the Power Electronics, Machines and Control Group at the University of Nottingham and in the Department of Electric Machines, Drives and Automation at the University of Zagreb. Her current research interests include design and control of power electronic converters for enhanced power quality and modelling, stability analysis and control of power electronics dominated micro-grids.